remote sensing

MDPI

Supplementary materials

InSAR-based mapping to support decision-making after an earthquake

Marta Béjar-Pizarro, José A. Álvarez Gómez, Alejandra Staller, Marco P. Luna, Raúl Pérez-López, Oriol Monserrat, Kervin Chunga, Aracely Lima, Jorge Pedro Galve, José J. Martínez Díaz , Rosa María Mateos, and Gerardo Herrera

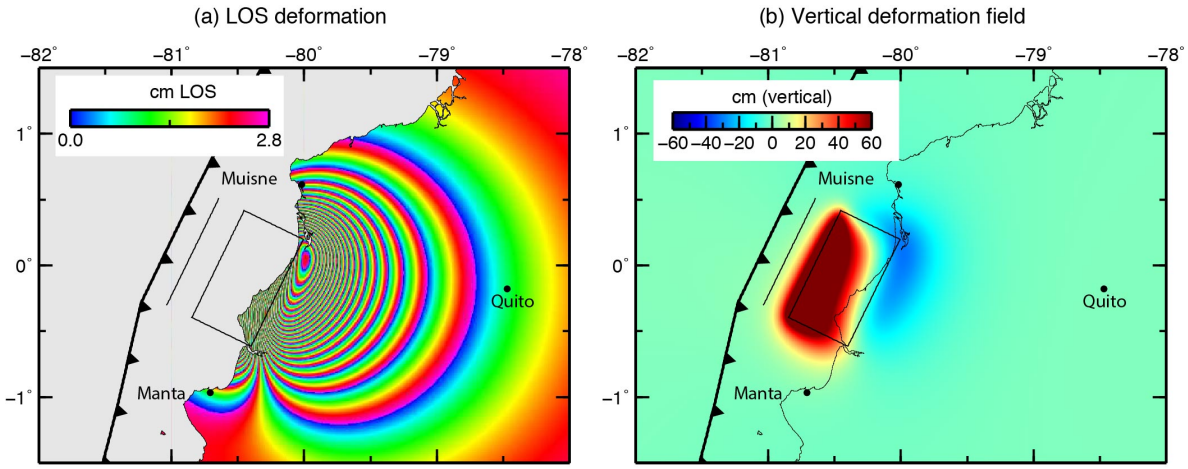

Figure S1. Ground deformation predicted by a uniform-slip model estimated using the expressions given by Okada (1985). Figure (a) shows the LOS deformation predicted by the model and figure (b) shows the vertical deformation predicted by the model (blue subsidence and red uplift). The modelled fault plane is shown as a black rectangle with the geometry of the Global CMT, uniform slip 3 m, length 100km and width 60 km.

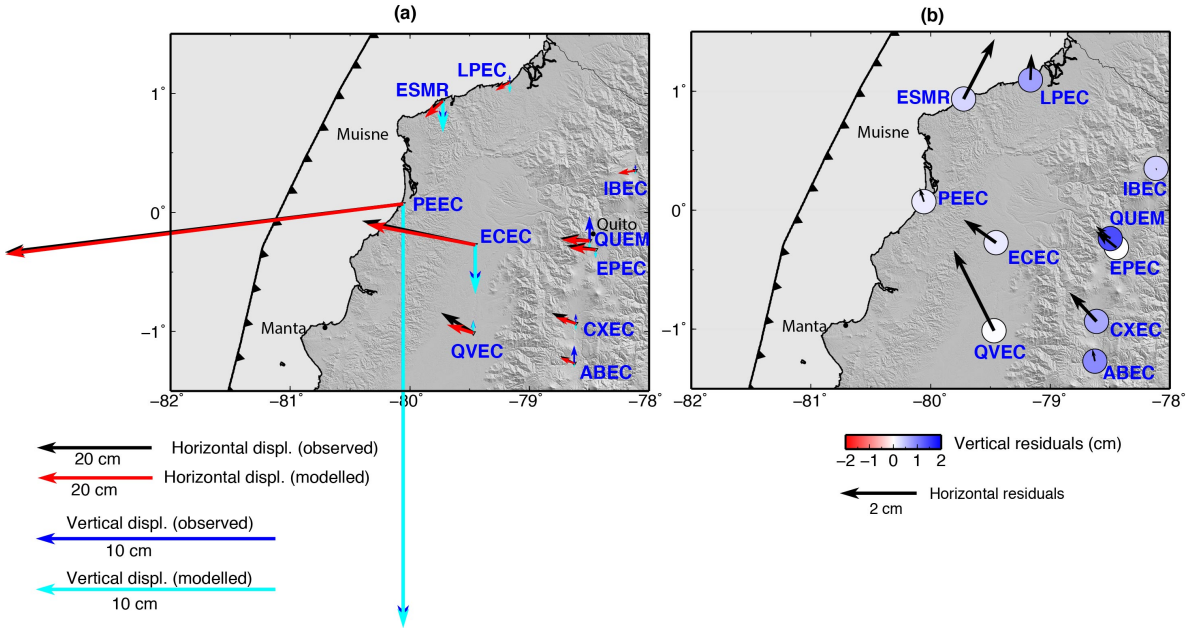

Figure S2. (a) Comparison between observed and modeled GPS displacements. Black and red arrows represent observed and modelled horizontal displacements respectively. Blue and cyan arrows represent observed and modelled vertical displacements respectively; **(b)** GPS residuals: black arrows indicate horizontal residuals and coloured circles represent vertical displacements.

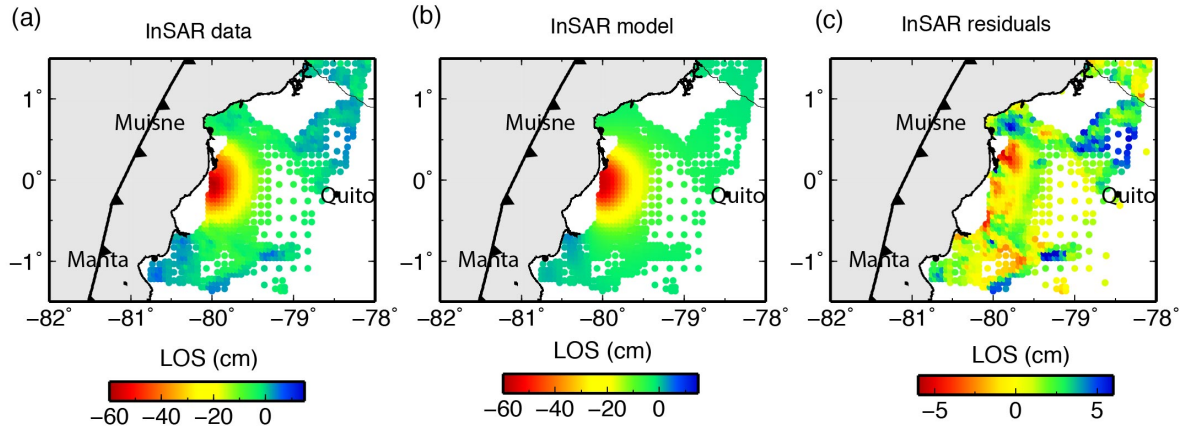

Figure S3. (a) InSAR deformation field; **(b)** InSAR displacements from our best variable-slip model; **(c)** InSAR residuals.

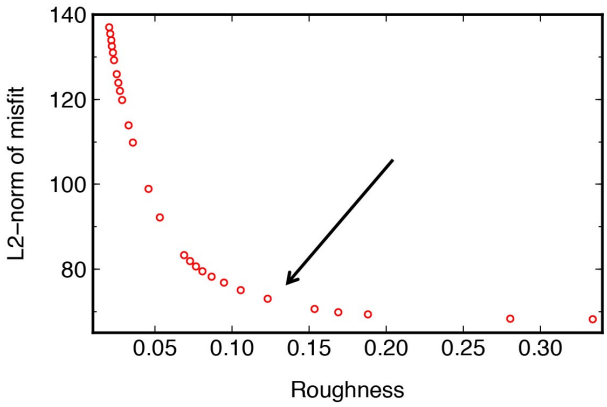

Figure S4. Trade-offs between L2 norm of least squares inversion misfit and model roughness for the coseismic models. The black arrows indicate the selected model.

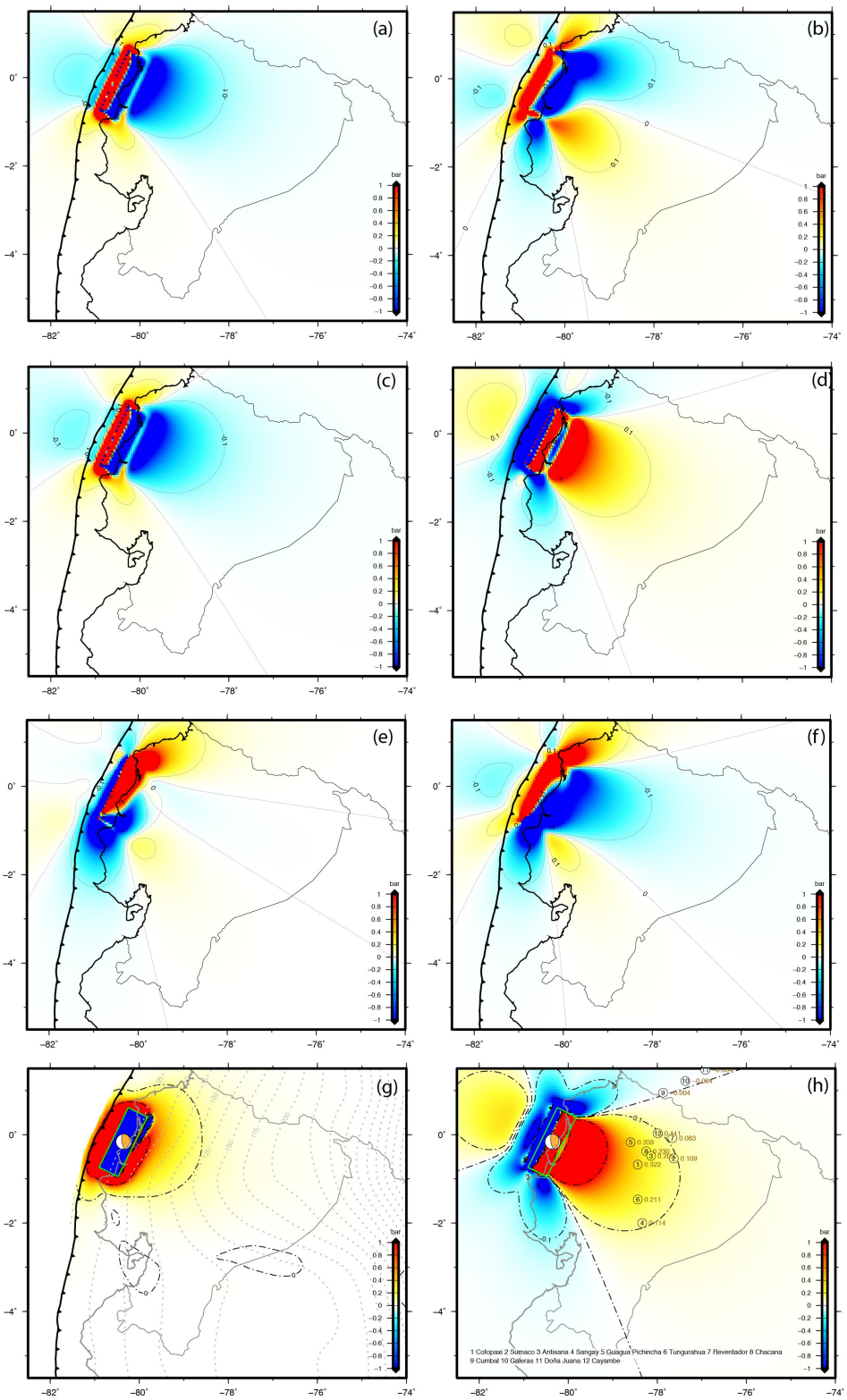

Figure S5. Coulomb failure stress changes induced by the 2016, Mw 7.8 Pedernales earthquake using the Global CMT focal mechanism. Maps (a-f) show different faults sets with the following strike/dip/rake: (a) 15/35/90; (b) 45/85/180; (c) 195/35/90 (d) 230/75/-90; (e) 110/75/-90; (f) 320/89/0; (g) Coulomb failure stress change on the subduction interface; (h) Coulomb failure stress changes on the volcanoes, indicated by black numbers: 1-Cotopaxi, 2-Sumaco, 3-Antisana, 4-Sangay, 5-Guagua Pichincha, 6-Tungurahua, 7-Reventador, 8-Chacana, 9-Cumbal, 10-Galeras, 11-Doña Juana, 12-Cayambe.

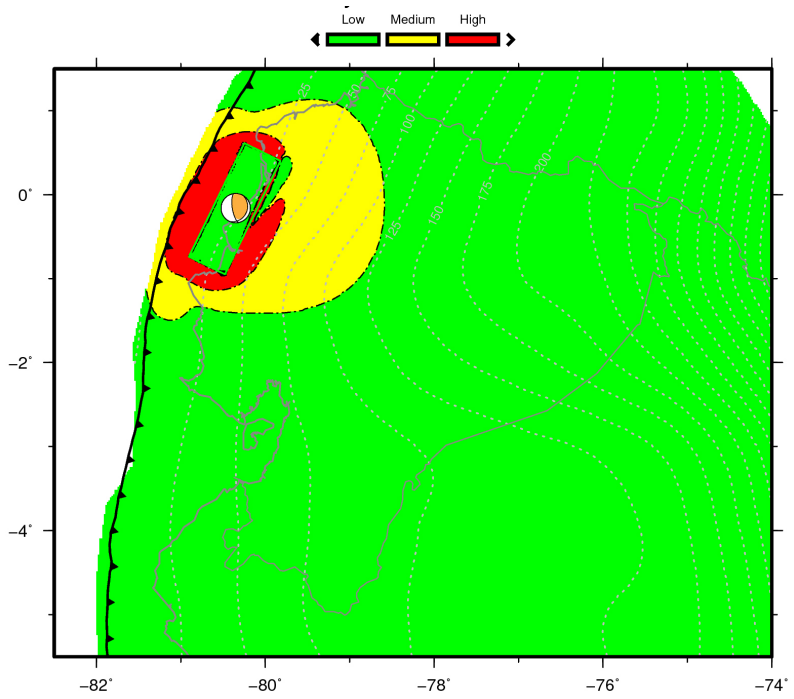

Figure S6. Map of potentially activated areas of the subduction interface using as earthquake source the Global CMT focal mechanism. The colour scale shows the level of potential activation of the subduction interface by the Pedernales earthquake. Green (low level) indicates areas with $\Delta CFS <$ 0.1 bar, yellow (medium level) indicates areas with 0.1 bar $\leq \Delta CFS \leq$ 1 bar and red (high level) indicates areas with $\Delta CFS >$ 1 bar. 25-km slab isodepth contour from [1] are indicated by the grey dashed lines.

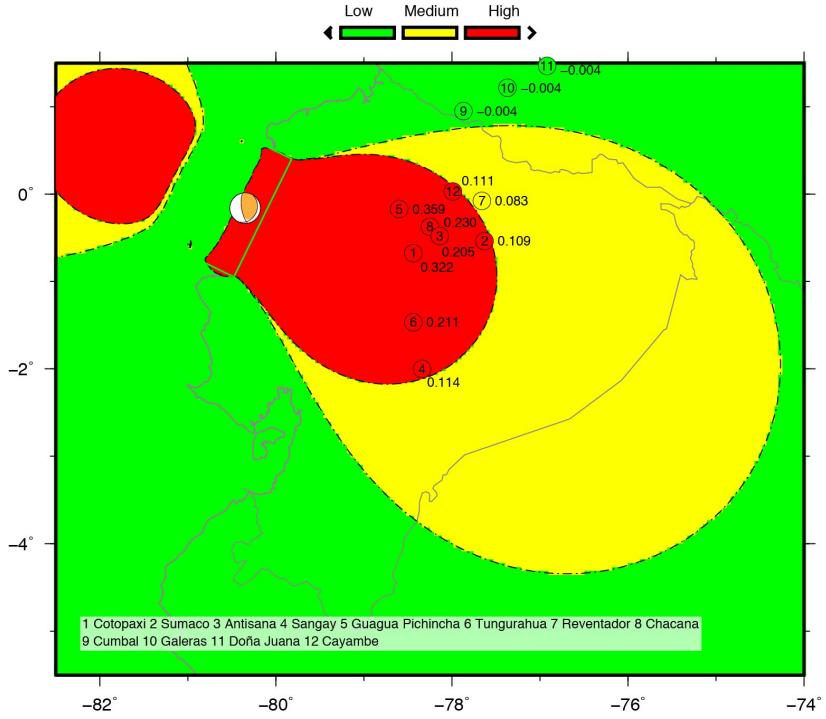

Figure S7. Map of potentially activated volcanoes using as earthquake source the Global CMT focal mechanism. Circled numbers indicate the Holocene volcanoes from http://volcano.si.edu/search_volcano.cfm. Colours indicate the level of potential activation of the volcano by the Pedernales earthquake, which depends on the value of the induced normal stress change ($\Delta\sigma$) on the volcano magma pathway. Green (low level) indicates volcanoes with $\Delta\sigma <$ 0.01

bar, yellow (medium level) indicates volcanoes with 0.01 bar ≤ $\Delta\sigma$ ≤ 0.1 bar and red (high level) indicates volcanoes with $\Delta\sigma$ > 0.1 bar.

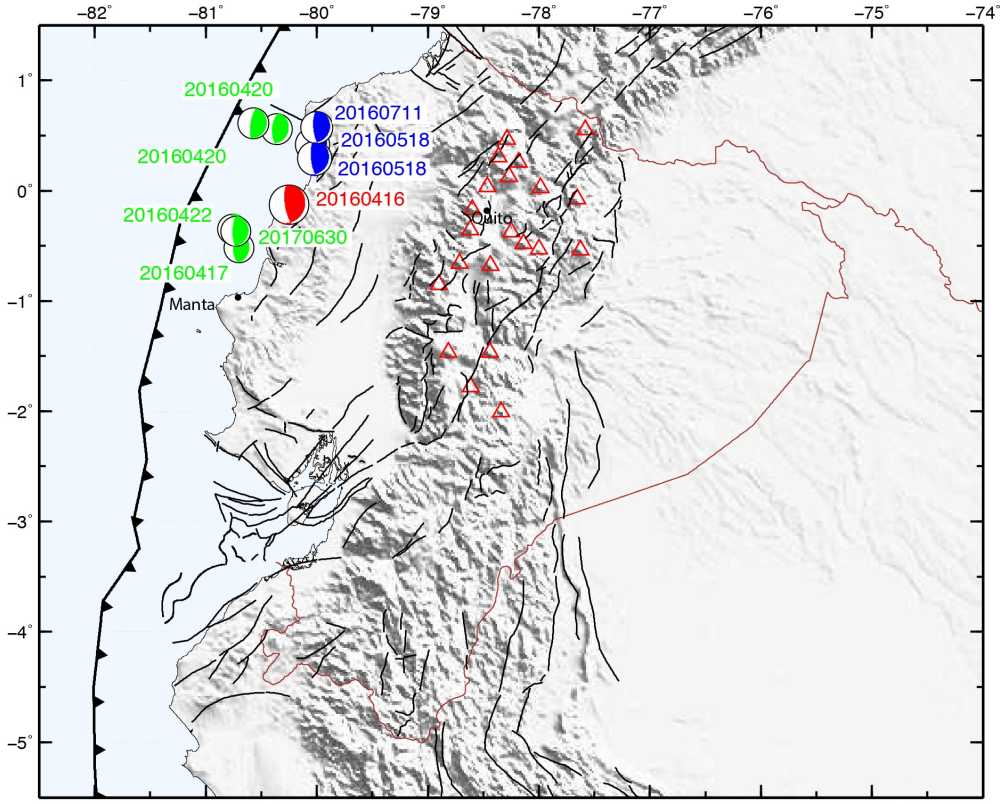

Figure S8. Global CMT focal mechanism of seismic events with Mw ≥ 6 occurred in the period April 16th 2016 – February 18th 2018. The Pedernales mainshock is represented in red and the three largest aftershocks, with Mw 6.3, 6.7 and 6.9, are represented in blue.

Table S1. Differences between GPS coseismic displacements and GPS coseismic displacements plus postseismic displacement during a period ranging between 2 to 6 days after the earthquake. The exacta period covered by each GPS site is indicated in column 4. All measures are in mm.

Site	lat	lon	Period	DEast	DNorth	DUp
ABEC	-1.269	-78.628	16-22 April	1.73	0.28	0.61
ALEC	-2.202	-78.847	16-22 April	0.25	-1.38	-0.11
BHEC	-1.798	-79.531	16-22 April	1.41	-2.56	2.59
CHEC	-0.339	-77.814	16-22 April	2.56	-1.05	3.9
COEC	0.716	-77.787	16-22 April	1.8	-1.04	0.59
CUEC	-2.883	-79.002	16-22 April	-0.04	-1.3	-1.45
CXEC	-0.935	-78.615	16-22 April	3.65	-2.27	1.87
ECEC	-0.272	-79.452	16-22 April	9.58	-2.11	0.82
EPEC	-0.315	-78.446	16-22 April	4.89	-1.51	-2.3
EREC	-1.671	-78.651	16-22 April	1.38	-2	2.16
ESMR	0.935	-79.724	16-18 April	2.58	-0.89	1.9
GUEC	-2.272	-79.904	16-22 April	-1.31	0.62	-3.3
IBEC	0.350	-78.116	16-18 April	2.19	-1.57	-2.9
LJEC	-3.988	-79.199	16-22 April	1.28	-2.38	-0.78
LPEC	1.095	-79.164	16-22 April	1.12	-0.73	4.27
MAEC	-2.305	-78.118	16-22 April	-0.27	-0.61	-0.47
NJEC	-2.675	-79.621	16-22 April	-0.42	0.11	3.65

PJEC	-1.552	-80.425	16-22 April	1.89	3.23	9.11
PREC	-1.708	-77.963	16-22 April	2.41	-3.76	-3.66
QUEM	-0.237	-78.497	16-20 April	2.86	-2.75	-2.95
QVEC	-1.012	-79.470	16-22 April	5.6	-1.5	-0.82
RIOP	-1.651	-78.651	16-18 April	1.91	-2.27	-3.1
SEEC	-0.903	-89.615	16-22 April	1.05	-1.2	0.88
SIEC	-3.275	-79.315	16-22 April	-1.36	2.22	0.29
TNEC	-0.990	-77.816	16-22 April	0.63	-0.32	5.94

Table S2. Comparison between GPS coseismic displacements (projected onto the local LOS vector) and InSAR data (corrected from an linear ramp) for 7 GPS sites located within the area covered by the InSAR data. All measures are in cm. The root mean square (RMS) difference is 1.07 cm. .

Site	lon	lat	GPS_LOS	InSAR	Diff
ABEC	-78.628	-1.269	-0.449	-2.335	1.887
CXEC	-78.615	-0.935	-1.556	-1.933	0.377
EPEC	-78.446	-0.315	-2.726	-1.531	-1.195
QUEM	-78.497	-0.237	-1.68	-1.257	-0.423
QVEC	-79.47	-1.012	-2.483	-1.363	-1.12
ECEC	-79.452	-0.272	-12.932	-12.357	-0.575
ESMR	-79.724	0.935	-2.44	-3.488	1.048

Table S3. Classification of the 278 faults segments in Chunga (2010) into 6 fault sets. The strike/dip/rake values used for the Coulomb failure stress estimation on each family are shown. .

Fault type	strike	dip	rake
Thrust faults, E dipping	195	35	90
Thurst faults, W dipping	15	35	90
Normal faults	110	75	-90
Normal faults	230	75	-90
Right-lateral strike-slip faults	45	85	180
Left-lateral strike-slip faults	320	89	0

Table S4. Dip and Azimuth of magma paths of the five selected Ecuadorian volcanoes used for the estimation of the stress changes.

Volcano	Azimuth	Dip
Tungurahua [1]	N200°E	85°
Guagua Pichincha [2,3,4]	N214°E	89°
Reventador [5]	N225°E	70°
Sangay [6]	N45°E	89°
Cotopaxi [7,8]	N70°E	89°

[1] Molina et al. 2005; [2] García-Aristizabal et al. 2007, [3]Legrand 2002, [4]Morales 2016, [5] Tibaldi 2005, [6] Monzier et al. 1999, [7] Fiorini 2012, [8] Molina 2008

References

1. Hayes, G. P.; D. J. Wal;, R. L. Johnson. Slab1.0: A three-dimensional model of global subduction zone geometries. *J. Geophys. Res.* **2012**, 117, B01302, doi:10.1029/2011JB008524.
2. Chunga, Kervin (2010). Terremoti crostali e zonazione sismica dell'Ecuador attraverso l'integrazione dei dati geologici, sismologici e morfostrutturali. PhD thesis
3. Okada, Y., 1985. Surface deformation to shear and tensile faults in a half space, Bull. seism. Soc. Am., 75, 1135–1154.
4. Molina, I.; Kumagai, H.; Le Penneca,J.L; Halla, M. Three-dimensional P-wave velocity structure of Tungurahua Volcano, Ecuador, *Journal of Volcanology and Geothermal Research* **2005**, *147*, 144–156

5. Garcia-Aristizabala,A. et al. Seismic, petrologic, and geodetic analyses of the 1999 dome-forming eruption of Guagua Pichincha volcano, Ecuador. *Journal of Volcanology and Geothermal Research* **2007**, *161*, 333–351.
6. Legrand, D et al. Stress tensor analysis of the 1998–1999 tectonic swarm of northern Quito related to the volcanic swarm of Guagua Pichincha volcano, Ecuador. *Tectonophysics* **2002,** *344*, 15–36
7. Morales Rivera, A. M., F. Amelung, and P. Mothes. Volcano deformation survey over the Northern and Central Andes with ALOS InSAR time series. *Geochem. Geophys. Geosyst.*, **2016**, *17*, 2869-2883, doi:10.1002/2016GC006393.
8. Tibaldi, A. Volcanism in compressional tectonic settings: Is it possible? *GEOPHYSICAL RESEARCH LETTERS* **2005**, *32*, L06309, doi:10.1029/2004GL021798
9. Monzier, M. et al. Sangay volcano, Ecuador: structural development, present activity and petrology. *Journal of Volcanology and Geothermal Research* **1999**, *90*, 49-79.
10. Fiorini, E.; Tibaldi, A. Quaternary tectonics in the central Interandean Valley, Ecuador: Fault-propagation folds, transfer faults and the Cotopaxi Volcano. *Global and Planetary Change* **2012**, *90–91*, 87–103
11. Molina, I. et al. Source process of very-long-period events accompanying long-period signals at Cotopaxi Volcano, Ecuador. *Journal of Volcanology and Geothermal Research* **2008**, *176*, 119–133